

Dosimetric comparison between volumetric modulated arc therapy planning techniques for prostate cancer in the presence of intrafractional organ deformation

Maria Varnava^{1,*}, Iori Sumida¹, Michio Oda², Keita Kurosu², Fumiaki Isohashi¹, Yuji Seo¹, Keisuke Otani¹ and Kazuhiko Ogawa¹

¹Department of Radiation Oncology, Osaka University Graduate School of Medicine, 2-2 (D10) Yamadaoka, Suita, Osaka, 565-0871, Japan

²Department of Medical Technology, Osaka University Hospital, 2-15 Yamadaoka, Suita, Osaka, 565-0871, Japan

*Corresponding author. Department of Radiation Oncology, Osaka University Graduate School of Medicine, 2-2 (D10) Yamadaoka, Suita, Osaka, 565-0871, Japan. Tel: +81-6-6879-3482; Fax: +81-6-6879-3489; Email: mvarnava@radonc.med.osaka-u.ac.jp

(Received 14 June 2020; revised 24 September 2020; editorial decision 12 November 2020)

ABSTRACT

The purpose of this study was to compare single-arc (SA) and double-arc (DA) treatment plans, which are planning techniques often used in prostate cancer volumetric modulated arc therapy (VMAT), in the presence of intrafractional deformation (ID) to determine which technique is superior in terms of target dose coverage and sparing of the organs at risk (OARs). SA and DA plans were created for 27 patients with localized prostate cancer. ID was introduced to the clinical target volume (CTV), rectum and bladder to obtain blurred dose distributions using an in-house software. ID was based on the motion probability function of each structure voxel and the intrafractional motion of the respective organs. From the resultant blurred dose distributions of SA and DA plans, various parameters, including the tumor control probability, normal tissue complication probability, homogeneity index, conformity index, modulation complexity score for VMAT, dose–volume indices and monitor units (MUs), were evaluated to compare the two techniques. Statistical analysis showed that most CTV and rectum parameters were significantly larger for SA plans than for DA plans ($P < 0.05$). Furthermore, SA plans had fewer MUs and were less complex ($P < 0.05$). The significant differences observed had no clinical significance, indicating that both plans are comparable in terms of target and OAR dosimetry when ID is considered. The use of SA plans is recommended for prostate cancer VMAT because they can be delivered in shorter treatment times than DA plans, and therefore benefit the patients.

Keywords: blurred dose distribution; dose–volume histogram; intrafractional organ deformation; prostate cancer; treatment planning; volumetric modulated arc therapy

INTRODUCTION

One of the common techniques for treating prostate cancer is volumetric modulated arc therapy (VMAT). As compared with 3D conformal radiation therapy, VMAT can deliver a highly conformal dose to the target, while minimizing the dose delivered to the organs at risk (OARs) [1, 2]. Furthermore, it can produce equivalent or even better target dose coverage and normal tissue sparing than intensity-modulated radiation therapy (IMRT) [3, 4], while taking advantage of more efficient monitor units (MUs) and reduced treatment time [3–5].

The VMAT technique uses modulated photon beams by simultaneous adjustment of the dose rate, gantry rotation speed and shape of the multileaf collimator aperture [1, 4, 5]. Treatment modalities that modulate fluence, like VMAT, are more prone to dosimetric errors due to patient setup errors and internal organ motion [6–8]. Such errors can have a significant impact on the dose absorbed by the target or the OARs, possibly yielding insufficient irradiation of the target or excess irradiation of the normal tissues due to reduced geometric and dosimetric accuracies. The expected absorbed dose can be calculated

from the treatment planning system (TPS), and the resulting dose distributions are used to evaluate the deliverability of the plans. However, the evaluation is based on a single dose distribution, which shows the dose a patient would receive if that patient's setup and anatomy were the same throughout treatment as those during the planning computed tomography (CT) imaging. Therefore, after the completion of treatment, the real dose distributions may deviate from the expected dose distributions [9].

Errors in the patient setup or interfractional organ motion can be reduced prior to a treatment session using image guidance [7, 10–12]. Various studies have tried to improve target localization accuracy and to account for interfractional setup errors and organ motion [12, 13]. Intrafractional organ deformation is more complex; it can be thought of as the combination of the motion of organ voxels in any direction. Thus, it is more difficult to correct the associated errors with intrafractional deformation (ID) during a treatment session. Real-time monitoring, tracking and adaptation are necessary to correct such errors. Previous studies have examined intrafractional organ motion during prostate cancer radiotherapy by using 4D ultrasound [14] and by investigating the displacement of fiducial markers implanted in the prostate before and after a treatment session using an on-board kilovoltage imaging system (OBI; Varian Medical Systems, Palo Alto, CA, USA) [15]. Other studies have focused on evaluating intrafractional organ motion using cine magnetic resonance imaging (cine-MRI) [16–18] and the Calypso 4D localization system (Calypso Medical Technologies, Seattle, WA, USA) [19, 20] with electromagnetic markers implanted in the target tissue.

One method to account for ID would be to create a model for organ deformation and to incorporate it into the calculation of dose distributions so as to get a more accurate representation of the real distributions. Pommer *et al.* [21] created a random walk model for simulating the characteristics of the observed intrafractional motion of the prostate when considering only motion from treatment fractions without transient excursions during the first 5 min. Another study calculated blurred dose (D_{blurred}) distributions of the prostate clinical target volume (CTV), rectum and bladder in IMRT [22] by simulating ID using displacements of these structures, the concepts of a static dose (D_{stat}) cloud approximation [23] and a probability density function (PDF) [24].

ID should be considered in radiation therapy, especially for VMAT. Any organ changes could degrade the accuracy of the plan because of the high dose conformality and steep dose gradients of VMAT, resulting in non-optimal plans with insufficient target irradiation and increased complications of the OARs. When creating treatment plans, VMAT offers the option of delivering dose to the target in either a single arc (SA) or multiple arcs. For prostate cancer, SA or double-arc (DA) plans are usually generated. There have been various studies comparing plans for prostate cancer created using either an SA or a DA plan [1–3, 5, 25–27], but none of them considered ID. These studies focused on the dosimetric comparison between SA and DA plans based on the dose distributions generated from the TPS. Non-consideration of ID makes unclear which one of these two options would lead to a more accurate delivery of the treatment. Therefore, the aim of this study was to compare SA and DA treatment plans for prostate cancer after the incorporation of ID and determine whether SA or DA plans are superior in terms of target dose coverage and sparing of the OARs.

MATERIALS AND METHODS

CT simulation and contouring

This study was approved by our Institutional Review Board (Osaka University Ethics Committee, approval number 18129) and written consent was obtained from all patients. Data from 27 patients, who were treated for localized prostate cancer using VMAT between June 2017 and March 2018, were retrospectively analyzed. The mean age [standard deviation (SD)] of the patients at the start of the treatment was 71 (7) years.

Before treatment, planning CT images were acquired using either a 16-slice multi-detector row CT (Bright Speed Elite; GE Healthcare, Waukesha, WI, USA) or a 320-slice multi-detector row CT (Aquilion ONE™; Canon Medical Systems, Otawara, Tochigi, Japan). The CT images were acquired with a slice thickness of 2.5 or 2 mm and with patients in a supine position on a vacuum-formed cushion (Vac-Lok™ cushion; CIVCO Medical Solutions, Kalona, IA, USA).

The CTV, rectum and bladder were delineated on the CT images on the Eclipse TPS (version 13.7.29, Varian Medical Systems, Palo Alto, CA, USA). The CTV was defined as the sum of the prostate and the proximal seminal vesicles, plus 3 or 1 mm in the posterior direction in order to avoid the rectum. The rectum and bladder were delineated by a medical physicist with 5 years of experience, and the CTV was delineated by a radiation oncologist with 8 years of experience.

Treatment planning and optimization

Two sets of VMAT treatment plans, SA and DA plans, were created for each patient using the arc parameters shown in Table 1. A dosage of 78 Gy was applied in 39 fractions to cover 50% of the planning target volume (PTV), which was defined as the CTV plus 5 mm. The treatment plans were inversely optimized. The optimization parameters were kept constant between the SA and DA plans of each patient and were based on the dosimetric planning goals (Table 2). In this study, the optimization parameters used for each plan were the same as the ones used to optimize the plan of the actual treatment of the patient. After optimization, all plans were calculated using the Acuros XB algorithm (version 13.7.14, Varian Medical Systems, Palo Alto, CA, USA) in the Eclipse TPS with a calculation grid size of 1 mm. Optimization was performed separately for each plan. SA and DA plans were optimized only once, and no alterations of the weightings of the optimization parameters were made so as to make fair comparisons between SA and DA plans possible.

Intrafractional organ deformation

The incorporation of organ deformation into the calculation of dose distributions and the estimation of D_{blurred} distributions were performed by following the procedure described in Sumida *et al.* [22]. D_{blurred} distributions refer to the resulting dose distributions after the completion of treatment. We assumed that the patient setup error was already accounted for by image guidance in each treatment session, so we considered only ID over the treatment course. The DICOM RT files including the treatment plan, structure set and dose were exported from the Eclipse TPS and were imported into an in-house software developed using Delphi2007 (Borland Software Corporation, Austin, TX, USA) to introduce ID to the structures of interest (CTV, rectum and bladder). The dose distribution at this point

Table 1. Arc parameters used for creating SA and DA plans

Parameter	SA plan	DA plan (first arc/second arc)
Arc direction	Anticlockwise	Anticlockwise/clockwise
Gantry angle (start–stop)	179–181°	179–181°/181–179°
Collimator angle	5–30°	330–350°

Table 2. Dosimetric planning goals used for designing treatment plans

Structure	Planning goal
CTV	$D_{95\%} \geq 74.1$ Gy
Rectum	$V_{40\text{Gy}} < 35\%$, $V_{65\text{Gy}} < 17\%$
Bladder	$V_{40\text{Gy}} < 50\%$, $V_{65\text{Gy}} < 25\%$

$D_{xx\%}$ = dose incident on xx% structure volume, $V_{xx\text{Gy}}$ = %volume of structure receiving a dose of xx Gy.

is referred to as the D_{stat} distribution because it is the distribution before considering ID, i.e. the dose distribution as calculated from the TPS. The software can create a probability dose distribution to each voxel of each structure based on a motion PDF. It was assumed that the motion PDF has three components, including axes of motion in the left–right (LR), anterior–posterior (AP) and superior–inferior (SI) directions, and that the motion probability was based on random organ deformations. The real motion distribution of the organs is unknown and can be affected by various factors, including respiration. However, according to the central limit theorem, even a non-uniform distribution will converge towards a Gaussian shape after a great number of fractions. Previous studies investigated the motion of the diaphragm under the influence of respiration [28, 29]. George *et al.* reported that the motion of the diaphragm tends to have a normal distribution when considering the respiration effect over multiple fractions for a single patient or when considering multiple fractions for all patients combined [28]. Rit *et al.* observed that the variability of the respiratory cycle over 2 min, which is similar to the treatment time of DA plans, is close to a skew normal distribution. Organs that have fewer mobile points than the diaphragm are expected to exhibit less asymmetry because the random baseline variations will dominate the probability density function [29]. Therefore, we assumed that the random deformations of the prostate, rectum and bladder over all 39 treatment fractions follow a normal distribution. Even though the prostate is known to move spontaneously [18, 30], by observing the overall dosimetric effect of ID through the whole treatment course of VMAT, spontaneous prostate movements will have a small dosimetric effect and can thus be neglected. Our proposed method, though, is not suitable for stereotactic or hypofractionated treatments, in which case the dosimetric effect of such prostate movements is great.

Amplitudes of the motion for the prostate, rectum and bladder during treatment in the LR, AP and SI directions have been reported in previous studies [31–33]. Two SDs of the reported motion of each organ were assumed to be the magnitude of ID and were used as

inputs in our software to introduce ID to the CTV, rectum and bladder (Table 3).

In order to consider ID, the number of times each organ (prostate, rectum and bladder) moves in a specific amount of time was necessary. From the results of a previous study, it was determined that the prostate position varied about 76 times in 4 min [16]. Furthermore, SA and DA plans usually have treatment times of 1 and 2 min, respectively. By taking these observations into account, we estimated that the prostate will move about 750 and 1500 times during the whole treatment course (39 fractions) of SA and DA plans, respectively. Since there have been no previous studies reporting data about the number of variations of the rectum and bladder positions in a specific period of time, we assumed that both OARs have the same number of variations as the prostate. Therefore, to calculate the D_{blurred} distributions for the CTV, rectum and bladder in the presence of ID, motion was introduced independently to each structure voxel. This was achieved by altering the location of the dose grid of each structure in the original dose cloud distribution, which was kept static, to fulfill the normal distribution criterion, as follows [22]:

$$D_{\text{blurred}}(x, y, z) = \sum_{i=1}^N D_{\text{stat}}(x + \sigma_i^{\text{LR}}, y + \sigma_i^{\text{AP}}, z + \sigma_i^{\text{SI}}) / N \quad (1)$$

where $D_{\text{blurred}}(x, y, z)$ is the mean value of the blurred dose at location (x, y, z) , with x , y and z corresponding to the LR, AP and SI directions, respectively. The location (x, y, z) is the same as the DICOM RT dose grid. The parameters σ_i^{LR} , σ_i^{AP} and σ_i^{SI} are the probable i^{th} location shifts in the LR, AP and SI directions (Table 3), respectively, with the locations randomly changed $N = 750$ times for SA plans and $N = 1500$ times for DA plans, based on the normal distribution. Figure 1 shows an example of the dose distribution before (D_{stat}) and after introducing ID (D_{blurred}) to the CTV in an SA plan.

Radiobiological evaluation

In order to compare SA and DA plans, various parameters were evaluated, including the generalized equivalent uniform dose (gEUD), tumor control probability (TCP), normal tissue complication probability (NTCP) and modulation complexity score for VMAT (MCSv).

The gEUD was calculated for each structure according to the Niemierko's phenomenological equation given by [34, 35]:

$$\text{gEUD} = \left(\frac{1}{N} \sum_{i=1}^N (D_i^a) \right)^{\frac{1}{a}} \quad (2)$$

where N is the number of voxels of each structure, each voxel receiving dose D_i in Gy, and a is a parameter specific to the tumor or normal tissue that describes the dose–volume effect. The TCP was calculated using

Table 3. ID magnitudes for the structures in each direction

Structure	ID magnitude (2 SDs, mm)			Study reference
	LR direction	AP direction	SI direction	
CTV	6	8	6	[31]
Rectum	6	10	0	[32]
Bladder	5	8	6	[33]

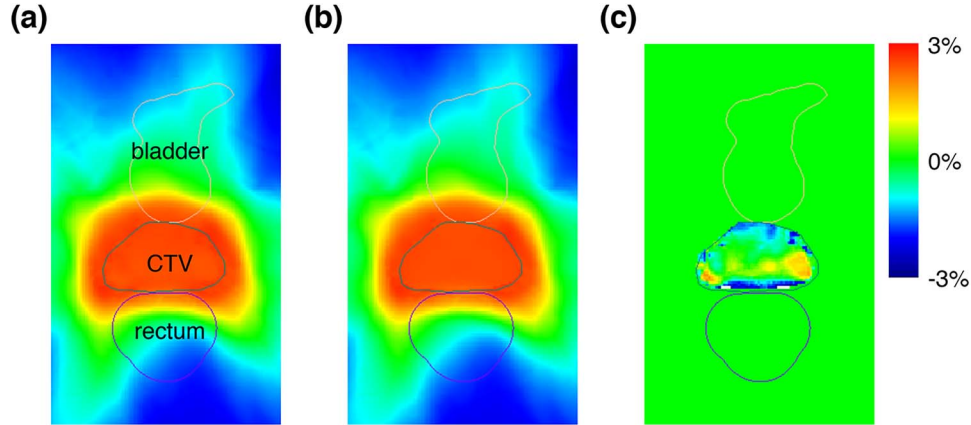


Fig. 1. Dose distributions of an SA plan. (a) The dose distributions as obtained from the TPS before introducing ID. (b) The D_{blurred} distributions after introducing ID to the CTV. (c) The subtraction image derived from (b) – (a).

the Niemierko EUD-based model given by the following equation [34, 36]:

$$\text{TCP} = \frac{1}{1 + \left(\frac{\text{TCD}_{50}}{\text{gEUD}}\right)^{4\gamma_{50}}} \quad (3)$$

where TCD_{50} is the dose needed to control 50% of the tumor when the tumor is homogeneously irradiated, and γ_{50} is a unitless parameter that is specific to the tumor and describes the slope of the dose–response curve. The individual voxel NTCP (P) was calculated using the relative seriality model [37], as follows:

$$P(D_i) = 2^{-e^{\gamma_{50}\left(1 - \frac{D_i}{D_{50}}\right)}} \quad (4)$$

where D_{50} refers to the tolerance dose that would produce a 50% complication rate at a specific time interval (e.g. 5 years) [38]. By considering the functional architecture of the organs, the NTCP was evaluated using the following equation [37]:

$$P = \left\{1 - \prod_1^n [1 - P(D_i)^s]^{\Delta v_i}\right\}^{\frac{1}{s}} \quad (5)$$

where n is the number of sub-volumes in the organ, and s is the relative seriality parameter, which ranges between 0 for parallel organs and 1 for serial organs. The parameter Δv_i is defined as v_i/V , where v_i is the sub-volume in the differential dose–volume histogram (DVH) and V is the

total volume of the organ. Table 4 shows the radiobiological parameters used for evaluating the gEUD, TCP and NTCP of the structures of interest.

The MCSv is a parameter that evaluates the complexity of VMAT plans. It was calculated based on the method described by Masi *et al.* [43], who modified the modulation complexity score for step-and-shoot IMRT proposed by McNiven *et al.* [44] to make it applicable for VMAT. The MCSv can take values in the range 0–1, with 1 showing no modulation, and thus no complexity. For example, a plan with $\text{MCSv} = 1$ would correspond to an arc with a fixed rectangular aperture with no leaves moving during the arc motion. VMAT plans with increased modulation have decreased MCSv.

Besides the parameters described above, dose–volume indices, the CTV homogeneity index (HI), the CTV conformity index (CI) and MUs were also used for comparing SA and DA plans.

The HI and CI were evaluated based on the definitions given by the International Commission on Radiation Units and Measurements (ICRU) Report 83 [45] and ICRU Report 62 [46], respectively:

$$\text{HI} = \frac{D_{2\%} - D_{98\%}}{D_{50\%}} \quad (6)$$

$$\text{CI} = \frac{V_{\text{TV}}}{V_{\text{target}}} \quad (7)$$

The $D_{2\%}$, $D_{98\%}$ and $D_{50\%}$ indices represent the doses received by 2, 98 and 50% of the CTV, respectively. V_{TV} refers to the treated volume, which is the volume enclosed by the 95% isodose lines, while V_{target} refers to the volume of the target. Based on ICRU Report 62,

Table 4. Radiobiological parameters used to calculate the gEUD, TCP and NTCP

Structure	a	TCD ₅₀ /D ₅₀ (Gy)	γ 50	s	Clinical endpoint	Study reference
CTV	-13	67.5	2.2	-	Local control	[39, 40]
Rectum	8.33	83.1	1.69	0.49	Grade 2 rectal bleeding	[39, 41]
Bladder	2	80	3	0.18	Symptomatic contracture	[39, 42]

Table 5. Comparison of MUs and MCSv between SA and DA plans; data are presented as mean ± SD

Parameter	SA plans	DA plans	P -value
MUs	550 ± 53	574 ± 52	<0.001*
MCSv	0.19 ± 0.03	0.18 ± 0.03	<0.001*

* P -values that indicate statistically significant differences.

V_{target} corresponds to the PTV. However, for comparing SA and DA plans, we considered only the CTV and not the PTV. Therefore, in our study, V_{target} corresponds to the CTV, while V_{TV} corresponds to the volume covered by at least 74.1 Gy since the prescription dose was 78 Gy.

Statistical analysis

Statistical analyses were performed using R software (version 3.5.0, Foundation for Statistical Computing, Vienna, Austria). The Shapiro–Wilk test was used to test the normality of the data. To investigate for differences between SA and DA plans, the two-tailed paired t-test or the Wilcoxon signed-rank test was used as appropriate. These tests were also used to investigate the effect ID has on SA and DA plans. A P -value of < 0.05 was considered statistically significant.

RESULTS

Table 5 shows the results after comparing the MUs and MCSv between SA and DA plans. Significant differences were found in both the MUs and MCSv. SA plans had fewer MUs than DA plans, whereas SA plans had larger MCSv, indicating less complexity and modulation than DA plans.

The plan parameters of SA and DA plans before and after introducing ID, i.e. the plan parameters of the D_{stat} and D_{blurred} distributions, are summarized in Supplementary Table S1, see online supplementary material. Statistical analysis of the dose–volume indices and radiobiological parameters of the structures of interest showed that most indices and parameters had statistically significant differences between the D_{stat} and D_{blurred} distributions of SA and DA plans (Supplementary Table S1). For both plans, the plan parameters of the D_{stat} distribution were larger overall than those of the D_{blurred} distribution. On the other hand, comparisons of the D_{blurred} distributions of the structures of interest between SA and DA plans revealed that there were no significant differences found in any dose–volume indices and radiobiological parameters for the bladder, while most parameters exhibited significant differences for the CTV and rectum. All CTV indices and parameters except the CTV $D_{98\%}$ and CTV CI had significantly larger values for SA plans than for DA plans. Similarly, all rectum indices and parameters except

$V_{40\text{Gy}}$ also had significantly larger values for SA plans. For the D_{stat} distributions, there were significant differences between SA and DA plans in the rectum $V_{65\text{Gy}}$, rectum NTCP and all CTV parameters. Out of all the plan parameters, the rectum $D_{2\%}$ had the largest significant difference between the D_{stat} and D_{blurred} distributions in both SA and DA plans. The rectum $D_{2\%}$ also had the largest significant difference in the D_{blurred} distribution between SA and DA plans, while the rectum $V_{65\text{Gy}}$ had the largest significant difference in the D_{stat} distribution. Figure 2 shows a graphical representation of this result.

DISCUSSION

This paper aimed to incorporate ID into the calculation of dose distributions and compare SA and DA plans based on the target dose coverage and sparing of the OARs. Significant differences between SA and DA plans were found in almost all the CTV and rectum parameters after ID introduction. From these results, we deduced that SA plans provide better CTV dosimetry and conformity, whereas DA plans provide better rectal dosimetry and CTV homogeneity.

Previous studies have investigated the differences between SA and DA plans for prostate cancer. Similar to our study, some studies detected better rectal dosimetry for DA plans than for SA plans [5, 25, 27]. On the other hand, Sale and Moloney [1] and Wolff *et al.* [2] found no significant differences in the rectal dosimetry between SA and DA plans, while Kang *et al.* [3] found no significant differences in the rectum NTCP. Furthermore, a different study reported an increased rectum dose–volume index ($V_{70\text{Gy}}$) in DA plans [26].

With regard to the target, Sze *et al.* [5], Chow and Jiang [25] and Guckenberger *et al.* [26] showed that DA plans have better target homogeneity, which agrees with our results, and better target dose conformity and coverage, while Wolff *et al.* [2] showed no significant differences in the target dosimetry. Moreover, one study reported no significant differences for the TCP [3].

In our study, no statistically significant differences were observed in any bladder parameters. This result is consistent with previous reports that found no significant differences in bladder dose–volume indices and NTCP between SA and DA plans [1, 3, 5]. Other studies, though, found better bladder dosimetry for DA plans [25–27].

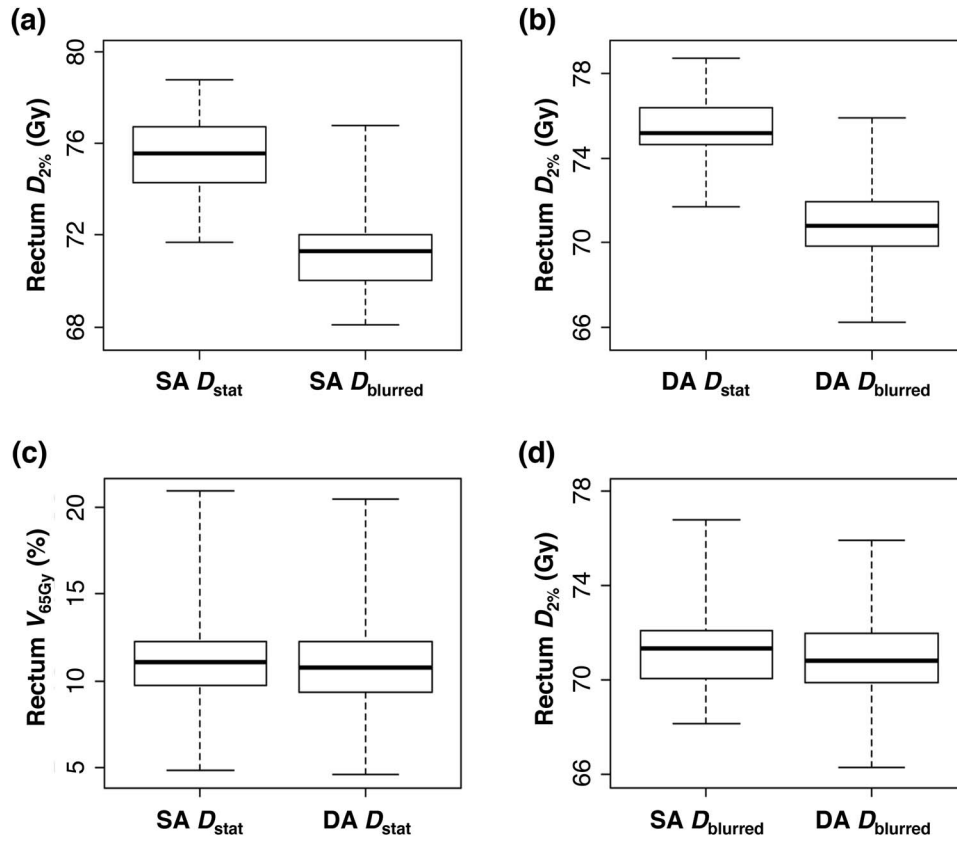


Fig. 2. Boxplots of the plan parameters that had the largest significant difference (a) between the D_{stat} and $D_{blurred}$ distributions of SA plans (rectum $D_{2\%}$), (b) between the D_{stat} and $D_{blurred}$ distributions of DA plans (rectum $D_{2\%}$), (c) in the D_{stat} distribution between SA and DA plans (rectum V_{65Gy}), and (d) in the $D_{blurred}$ distribution between SA and DA plans (rectum $D_{2\%}$). $D_{xx\%}$ = dose incident on $xx\%$ structure volume, V_{xxGy} = %volume of structure receiving a dose of xx Gy.

Inconsistencies between our findings with previously published research can be mainly attributed to the consideration of ID in our study. Statistically significant dosimetric differences were observed between the plans in our study before and after the incorporation of ID ($P < 0.05$). Different planning designs, such as planning goals, planning strategies, arc parameters, optimization parameters, target definitions and PTV margins, may also affect the dosimetric results and constitute a reason for the inconsistencies.

Despite the inconsistencies between studies, we found that our significant differences were in general smaller in magnitude than those in the above-mentioned studies. This could be explained from the dose blurring and interplay effect caused by ID [47]. Dose blurring effect is the reduction of the dose delivered to a point in a structure due to the motion of this point. Interplay effect is the dosimetric effect caused by the relative motion of the structures between the leaves and the treatment region. Both the dose blurring and interplay effects yield a non-uniform dose distribution delivered to the moving structures. By considering the mean dose delivered across all fractions, as in our study, the dosimetric differences caused by these two effects become smaller [47] compared with when ID is not considered. This is also the reason most of the plan parameters of the D_{stat} distributions were larger than those of the $D_{blurred}$ distributions in both SA and DA plans.

Our results show that the significant differences found in the $D_{blurred}$ distributions between SA and DA plans were very small, with the largest difference being <0.6 Gy for the rectum $D_{2\%}$ (Supplementary Table S1). A previous study found a statistically significant difference in the mean dose of the small bowel between IMRT and VMAT DA plans for prostate cancer [27]. This difference was 1.4 Gy, which is larger than our 0.6 Gy difference, and the indices between the two plans were considered comparable. Furthermore, our CTV $D_{2\%}$, the index with the largest significant difference among the CTV indices, had a difference of 0.2 Gy, with the $D_{2\%}$ of SA plans being 0.2% higher than that of DA plans. Dose differences should be interpreted in the context of the total uncertainty in radiation therapy that is clinically accepted. The International Commission on Radiation Protection [48] has reported an estimated standard uncertainty of 5% in a clinical setup when considering the uncertainty in the complete workflow (uncertainty in beam calibration, relative dosimetry, dose calculations and dose delivery). Our CTV $D_{2\%}$ difference of 0.2% only makes up for a small fraction of the total uncertainty. Additionally, the bladder NTCP had no significant differences between SA and DA plans, while the significant differences for the TCP and rectum NTCP were $<0.1\%$. Kang *et al.* [3] reported a 0.2% difference in the rectum NTCP results in radiobiological outcomes that have no difference between the various

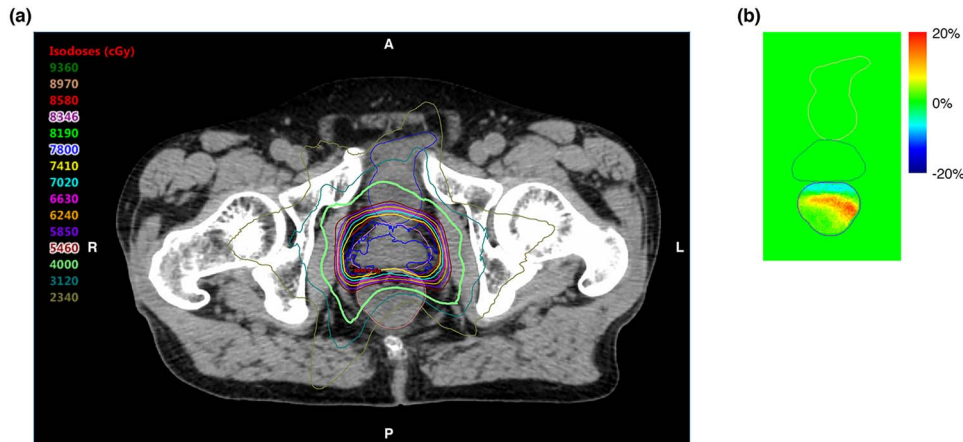


Fig. 3. Effect of ID on the low doses delivered to the rectum (≤ 40 Gy). (a) D_{stat} distributions of an SA plan as obtained from the TPS. The bold light-green line represents the 40-Gy isodose line. (b) Dose differences between the D_{blurred} distributions after introducing ID to the rectum and the D_{stat} distributions in (a).

VMAT plans investigated. Our TCP and rectum NTCP differences were much smaller than 0.2%, meaning that both SA and DA plans result in similar tumor control and OAR complications. In addition, the significant differences observed in the MCSv had a magnitude of 0.01, indicating that even though SA and DA plans have statistically different complexities, their complexities are similar. Therefore, we deduced that SA and DA plans are comparable in terms of target dose coverage, sparing of the OARs and plan complexity.

For the D_{stat} distributions, significant differences were found in all CTV parameters, the rectum $V_{65\%}$ and rectum NTCP between SA and DA plans. Almost all indices had significantly larger values for SA plans than for DA plans. This implies that the D_{stat} SA plans have better CTV dosimetry than the D_{stat} DA plans, while D_{stat} DA plans have better rectal dosimetry [5, 25, 27]. These are consistent with the findings of the D_{blurred} distributions. Furthermore, the D_{stat} SA and D_{stat} DA plans are comparable in terms of the bladder dosimetry, which agrees with previous studies [1, 3, 5]. It can be deduced that D_{stat} SA and DA plans exhibit the same trend as D_{blurred} plans.

The rectum $V_{40\text{Gy}}$ was the only dose–volume index that increased after applying ID. As can be seen in Fig. 3a, the low-dose isodose lines (≤ 40 Gy) have steep gradients around the rectum. The rectum moves in the LR and AP direction (Table 3). The shape of the low-dose isodose lines and the shift of the rectal wall causes an excess of the planned dose in the rectal posterior region after the completion of treatment (Fig. 3b), which results in the observed increase in the rectum $V_{40\text{Gy}}$. The remaining dose–volume indices decreased after the introduction of ID probably due to the dose blurring and interplay effects that were previously discussed.

Analysis of our data revealed the importance of considering ID during plan quality evaluation. In general, when a dose–volume constraint was met before ID introduction, the constraint was also met after ID introduction since the values of the dose–volume indices decreased. This was not the case for the rectum $V_{40\text{Gy}}$ constraint, which was met in 20 D_{stat} SA and 20 D_{stat} DA plans, whereas it was met in 14 D_{blurred} SA plans and 13 D_{blurred} DA plans. This indicates that the unfulfilled

rectum $V_{40\text{Gy}}$ constraint would have remained undetected in 6 SA and 7 DA plans without ID consideration. Relying only on the dose distributions created by the TPS may lead to the wrong conclusions about the real dose distributions, and result in accepting treatment plans that do not fulfil all the dose–volume constraints, without being aware of it. Introducing ID to the plans leads to more realistic dose distributions. Therefore, considering ID during plan quality evaluation is important so as to confirm that all dose–volume constraints are met and avoid any unnecessary complications. Furthermore, the fact that the $V_{40\text{Gy}}$ constraint was met in a different number of SA and DA plans in both D_{stat} and D_{blurred} distributions shows that even though the differences between SA and DA plans are small, they could lead to different fulfilled dose–volume constraints, which would not always be apparent without ID consideration.

In our study, the same dose–volume constraints were used for creating SA and DA plans for each patient. It could be argued that using the same constraints would lead to similar plans. In a previous study, three institutions created IMRT plans for a prostate cancer patient using the same contours [49]. Each institution used different optimization parameters and constraints to create the best possible IMRT plan. Even though the plan parameters were different, the resulting plans were similar with respect to dose–volume constraints, with greater variations in the DVHs of the OARs. This implies that plans created for the same patient will be similar regardless of the constraints used when aiming for a good quality plan. Tang *et al.* reported that transforming multiple-arc plans to SA plans in intensity-modulated arc therapy for five different sites resulted in similar plans [50]. Also, a different study created IMRT plans for head-and-neck cancer using 3, 5, 7 and 9 beams [51]. The constraints and weight factors were modified during optimization to control the progress of the DVH curves. Increasing the number of beams led to improved dosimetric results, while the plans created using 7 and 9 beams had similar dose distributions. It can be deduced that plans with multiple beams will yield similar dose distributions for the same patient regardless of the choice of dose–volume constraints. This is consistent with our results that SA and DA

plans are similar, as these plans can be described as plans with multiple beams.

During the radiobiological evaluation of the plans, dose-rate effects were not considered. It has been reported that considerable differences are apparent for dose rates in the range 0.1–100 cGy/min; some cell systems exhibit more cell sub-lethal damage for lower dose-rates, while other cell systems exhibit more damage repair [52]. However, there is no effect on cells for dose-rates in the range 100–1000 cGy/min [52]. A previous study that investigated the radiobiological effects of total body irradiation on the spinal cord showed that for dose rates > 50 cGy/min the effect is negligible for various fractionation schemes [53]. Another study reviewed the dose-rate effect on external beam radiation therapy and reported that for treatments using a dose of 1.8–2 Gy per fraction, the effect of dose rate is relatively small and is mainly influenced by the overall beam-on-time and not by the average linac dose rate nor by the instantaneous dose rate within the individual linac pulses [54]. On the other hand, Bewes *et al.* showed that besides treatment time, average dose rate also has different effects on the clonogenic cell survival: shorter treatment times and higher dose rates led to reduced cell survival [55]. In this study, the dose rates in the SA and DA plans had minimum/maximum values (mean \pm SD) of $425 \pm 60/600 \pm 0$ and $222 \pm 26/440 \pm 103$ MU/min, respectively. By taking into consideration the findings of previous research, it can be deduced that SA plans may possibly have better therapeutic gain than DA plans. The difference in therapeutic effect, though, would be relatively small.

The results of the current study lead to the same conclusion as published research: both SA and DA plans are similar and acceptable options for prostate cancer VMAT [1–3, 5, 25]. SA plans, which have shorter treatment times than DA plans, may be preferred [5], unless the dose–volume criteria are difficult to achieve [1, 25]. Previous studies, though, have only focused on the dose distributions as obtained from the TPS, whereas we introduced ID to the plans in order to obtain more accurate representations of the dose distributions. The fact that the conclusions of our study agree with the conclusions of previous studies strengthens the consensus that SA and DA plans are similar.

A limitation of this study is the fact that residual errors were not considered. After image guidance, residual geometric setup errors remain due to inaccuracies of the imaging system, the repositioning system and the intrafractional motion of the prostate [56]. The system-related setup errors have been reported to be <2 mm [56]. In this study, we focused only on organ deformation. A future study could also incorporate system-related residual errors so as to obtain an even more realistic representation of the dose distributions. Another limitation is the assumption that the magnitude of organ motion is the same as the magnitude of intrafractional organ deformation. During the actual treatment, this might not always be true, as movement of the voxels of an organ could lead to movement of the organ as a whole and not in deformation of the organ. Moreover, it was assumed that, in each direction, all voxels of an organ have the same motion magnitude. A previous study showed that the prostate has different motion magnitudes for different parts of the prostate in a specific direction [57]. From this, it can be deduced that the magnitude of the prostate deformation in one direction is not the same for all prostate voxels. The same thing most likely applies to all organs. Various studies used cine-MRI to investigate intrafractional organ motion for the prostate, bladder and

seminal vesicles in terms of time [16–18, 28, 57, 58]. Most of these studies identified dosimetric uncertainties arising from intrafractional organ motion and suggested the consideration of suitable strategies to account for the dosimetric uncertainties, such as control of the rectum and bladder filling [17, 57], the use of a rectal balloon [16] and the use of appropriate intrafractional organ margins [30, 58]. By following a similar method to these studies and their proposed strategies for controlling the rectum and bladder filling, it could be possible to determine ID for the organs (or structures) of interest for each patient during a treatment session and limit any volume variations in the OARs, which could degrade the performance of our model as volume variations were not considered during ID simulation. By using this ID, more accurate dose distributions could be estimated, and the dosimetric effect on SA and DA plans could be reassessed to confirm the reliability of our results. In addition, recent studies have attempted to monitor intrafractional organ motion and deformation using MRI-guided radiation therapy setups [59–61]. Similar to cine-MRI, such setups would enable determination of the ID of the target and OARs in various cancer sites. Based on the way the shape of an organ varies over time, a future study could investigate which arc angles in prostate cancer VMAT are least affected by ID, resulting in treatment plans that are not susceptible to ID and therefore are more accurate than SA and DA plans.

In conclusion, the evidence from this study points towards the idea that ID incorporation into the calculation of dose distributions is important for ensuring that all dosimetric planning goals are met. Moreover, our results indicate that SA and DA treatment plans for prostate cancer are comparable in terms of target and OAR dosimetry when ID is considered. SA plans, though, can be delivered in shorter treatment times than DA plans, leading to less patient discomfort and possibly better therapeutic gain. Thus, the use of SA plans, in combination with ID consideration during plan quality evaluation, is recommended so as to benefit patients.

SUPPLEMENTARY DATA

Supplementary data is available at *RADRES Journal* online.

CONFLICT OF INTEREST

None declared.

REFERENCES

1. Sale C, Moloney P. Dose comparisons for conformal, IMRT and VMAT prostate plans. *J Med Imaging Radiat Oncol* 2011;55:611–21.
2. Wolff D, Stieler F, Welzel G et al. Volumetric modulated arc therapy (VMAT) vs. serial tomotherapy, step-and-shoot IMRT and 3D-conformal RT for treatment of prostate cancer. *Radiother Oncol* 2009;93:226–33.
3. Kang SW, Chung JB, Kim JS et al. Optimal planning strategy among various arc arrangements for prostate stereotactic body radiotherapy with volumetric modulated arc therapy technique. *Radiol Oncol* 2017;51:112–20.
4. Otto K. Volumetric modulated arc therapy: IMRT in a single gantry arc. *Med Phys* 2008;35:310–7.

5. Sze HC, Lee MC, Hung WM et al. RapidArc radiotherapy planning for prostate cancer: Single-arc and double-arc techniques vs. intensity-modulated radiotherapy. *Med Dosim* 2012;37:87–91.
6. Azcona JD, Xing L, Chen X et al. Assessing the dosimetric impact of real-time prostate motion during volumetric modulated arc therapy. *Int J Radiat Oncol Biol Phys* 2014;88:1167–74.
7. Palombarini M, Mengoli S, Fantazzini P et al. Analysis of inter-fraction setup errors and organ motion by daily kilovoltage cone beam computed tomography in intensity modulated radiotherapy of prostate cancer. *Radiat Oncol* 2012;7:56.
8. Trofimov A, Rietzel E, Lu HM et al. Temporo-spatial IMRT optimization: Concepts, implementation and initial results. *Phys Med Biol* 2005;50:2779–98.
9. Langen KM, Jones DT. Organ motion and its management. *Int J Radiat Oncol Biol Phys* 2001;50:265–78.
10. Mc Parland NA. kV-cone beam CT as an IGRT tool in the treatment of early stage prostate cancer: A literature review. *J Med Imaging Radiat Sci* 2009;40:9–14.
11. McBain CA, Henry AM, Sykes J et al. X-ray volumetric imaging in image-guided radiotherapy: The new standard in on-treatment imaging. *Int J Radiat Oncol Biol Phys* 2006;64:625–34.
12. Willoughby TR, Kupelian PA, Pouliot J et al. Target localization and real-time tracking using the calypso 4D localization system in patients with localized prostate cancer. *Int J Radiat Oncol Biol Phys* 2006;65:528–34.
13. Boda-Heggemann J, Köhler FM, Küpper B et al. Accuracy of ultrasound-based (BAT) prostate-repositioning: A three-dimensional on-line fiducial-based assessment with cone-beam computed tomography. *Int J Radiat Oncol Biol Phys* 2008;70:1247–55.
14. Baker M, Behrens CF. Determining intrafractional prostate motion using four dimensional ultrasound system. *BMC Cancer* 2016;16:484.
15. Kron T, Thomas J, Fox C et al. Intra-fraction prostate displacement in radiotherapy estimated from pre- and post-treatment imaging of patients with implanted fiducial markers. *Radiation Oncol* 2010;95:191–7.
16. Vargas C, Saito AI, Hsi WC et al. Cine-magnetic resonance imaging assessment of intrafraction motion for prostate cancer patients supine or prone with and without a rectal balloon. *Am J Clin Oncol* 2010;33:11–6.
17. McBain CA, Khoo VS, Buckley DL et al. Assessment of bladder motion for clinical radiotherapy practice using cine-magnetic resonance imaging. *Int J Radiat Oncol Biol Phys* 2009;75:664–71.
18. Mah D, Freedman G, Milestone B et al. Measurement of intrafractional prostate motion using magnetic resonance imaging. *Int J Radiat Oncol Biol Phys* 2002;54:568–75.
19. Tong X, Chen X, Li J et al. Intrafractional prostate motion during external beam radiotherapy monitored by a real-time target localization system. *J Appl Clin Med Phys* 2015;16:51–61.
20. Langen KM, Willoughby TR, Meeks SL et al. Observations on real-time prostate gland motion using electromagnetic tracking. *Int J Radiat Oncol Biol Phys* 2008;71:1084–90.
21. Pommer T, Oh JH, Munck Af Rosenschöld P et al. Simulating intrafraction prostate motion with a random walk model. *Adv Radiat Oncol* 2017;2:429–36.
22. Sumida I, Yamaguchi H, Das IJ et al. Robust plan optimization using edge-enhanced intensity for intrafraction organ deformation in prostate intensity-modulated radiation therapy. *PLoS One* 2017;12:e0173643.
23. Craig T, Battista J, VanDyk J. Limitations of a convolution method for modeling geometric uncertainties in radiation therapy. I. the effect of shift invariance. *Med Phys* 2003;30:2001–11.
24. Bortfeld T, Jokivarsi K, Goitein M et al. Effects of intra-fraction motion on IMRT dose delivery: Statistical analysis and simulation. *Phys Med Biol* 2002;47:2203–20.
25. Chow JC, Jiang R. Prostate volumetric-modulated arc therapy: Dosimetry and radiobiological model variation between the single-arc and double-arc technique. *J Appl Clin Med Phys* 2013;14:3–12.
26. Guckenberger M, Richter A, Krieger T et al. Is a single arc sufficient in volumetric-modulated arc therapy (VMAT) for complex-shaped target volumes? *Radiation Oncol* 2009;93:259–65.
27. Yoo S, Wu QJ, Lee WR et al. Radiotherapy treatment plans with RapidArc for prostate cancer involving seminal vesicles and lymph nodes. *Int J Radiat Oncol Biol Phys* 2010;76:935–42.
28. George R, Keall PJ, Kini VR et al. Is the diaphragm motion probability density function normally distributed? *Med Phys* 2005;32:396–404.
29. Rit S, van Herk M, Zijp L et al. Quantification of the variability of diaphragm motion and implications for treatment margin construction. *Int J Radiat Oncol Biol Phys* 2012;82:e399–407.
30. Ghilezan MJ, Jaffray DA, Siewerdsen JH et al. Prostate gland motion assessed with cine-magnetic resonance imaging (cine-MRI). *Int J Radiat Oncol Biol Phys* 2005;62:406–17.
31. Maleike D, Unkelbach J, Oelfke U. Simulation and visualization of dose uncertainties due to interfractional organ motion. *Phys Med Biol* 2006;51:2237–52.
32. Scaife J, Harrison K, Romanchikova M et al. Random variation in rectal position during radiotherapy for prostate cancer is two to three times greater than that predicted from prostate motion. *Br J Radiol* 2014;87:20140343.
33. Tuomikoski L, Korhonen J, Collan J et al. Implementation of adaptive radiation therapy for urinary bladder carcinoma: Imaging, planning and image guidance. *Acta Oncol* 2013;52:1451–7.
34. Gay HA, Niemierko A. A free program for calculating EUD-based NTCP and TCP in external beam radiotherapy. *Phys Med* 2007;23:115–25.
35. Wu Q, Mohan R, Niemierko A et al. Optimization of intensity-modulated radiotherapy plans based on the equivalent uniform dose. *Int J Radiat Oncol Biol Phys* 2002;52:224–35.
36. Anbumani S, Arunai Nambi Raj N, Prabhakar GS et al. Quantification of uncertainties in conventional plan evaluation methods in intensity modulated radiation therapy. *J BUON* 2014;19:297–303.
37. Källman P, Agren A, Brahme A. Tumour and normal tissue responses to fractionated non-uniform dose delivery. *Int J Radiat Biol* 1992;62:249–62.

38. Emami B, Lyman J, Brown A et al. Tolerance of normal tissue to therapeutic irradiation. *Int J Radiat Oncol Biol Phys* 1991;21:109–22.
39. Sumida I, Yamaguchi H, Kizaki H et al. Novel radiobiological gamma index for evaluation of 3-dimensional predicted dose distribution. *Int J Radiat Oncol Biol Phys* 2015;92:779–86.
40. Cheung R, Tucker SL, Lee AK et al. Dose-response characteristics of low- and intermediate-risk prostate cancer treated with external beam radiotherapy. *Int J Radiat Oncol Biol Phys* 2005;61:993–1002.
41. Rancati T, Fiorino C, Gagliardi G et al. Fitting late rectal bleeding data using different NTCP models: Results from an Italian multi-centric study (AIROPROS0101). *Radiother Oncol* 2004;73:21–32.
42. Mavroidis P, Giantsoudis D, Awan MJ et al. Consequences of anorectal cancer atlas implementation in the cooperative group setting: Radiobiologic analysis of a prospective randomized in silico target delineation study. *Radiother Oncol* 2014;112:418–24.
43. Masi L, Doro R, Favuzza V et al. Impact of plan parameters on the dosimetric accuracy of volumetric modulated arc therapy. *Med Phys* 2013;40:071718-1–071718-11.
44. McNiven AL, Sharpe MB, Purdie TG. A new metric for assessing IMRT modulation complexity and plan deliverability. *Med Phys* 2010;37:505–15.
45. Prescribing ICRU. Recording, and reporting photon-beam intensity-modulated radiation therapy (IMRT). Special considerations regarding absorbed-dose and dose-volume prescribing and reporting in IMRT. ICRU report 83. *J ICRU* 2010;10:27–40.
46. ICRU. *Prescribing, recording, and reporting photon beam therapy (Supplement to ICRU Report 50)*. ICRU Report 62. Bethesda, MD: ICRU, 1999.
47. Seco J, Sharp GC, Turcotte J et al. Effects of organ motion on IMRT treatments with segments of few monitor units. *Med Phys* 2007;34:923–34.
48. ICRP. Prevention of accidents to patients undergoing radiation therapy. ICRP publication 86. *Ann ICRP* 2000;30:7–70.
49. Skala M, Holloway L, Bailey M et al. Australia-wide comparison of intensity modulated radiation therapy prostate plans. *Australas Radiol* 2005;49:222–9.
50. Tang C, Earl MA, Luan S et al. Converting multiple-arc intensity modulated arc therapy into a single arc for efficient delivery. *Int J Radiat Oncol Biol Phys* 2007;69:S673.
51. Samuelsson A, Johansson KA. Intensity modulated radiotherapy treatment planning for dynamic multileaf collimator delivery: Influence of different parameters on dose distributions. *Radiother Oncol* 2003;66:19–28.
52. Hall EJ, Brenner DJ. The dose-rate effect revisited: Radiobiological considerations of importance in radiotherapy. *Int J Radiat Oncol Biol Phys* 1991;21:1403–14.
53. Nevelsky A, Bar-Deroma R, Kuten A. Radiobiological effects of total body irradiation on the spinal cord. *Radiat Environ Biophys* 2009;48:385–9.
54. Ling CC, Gerweck LE, Zaider M et al. Dose-rate effects in external beam radiotherapy redux. *Radiother Oncol* 2010;95:261–8.
55. Bewes JM, Suchowerska N, Jackson M et al. The radiobiological effect of intra-fraction dose-rate modulation in intensity modulated radiation therapy (IMRT). *Phys Med Biol* 2008;53:3567–78.
56. Poulsen PR, Muren LP, Høyer M. Residual set-up errors and margins in on-line image-guided prostate localization in radiotherapy. *Radiother Oncol* 2007;85:201–6.
57. Ogino I, Kaneko T, Suzuki R et al. Rectal content and intrafractional prostate gland motion assessed by magnetic resonance imaging. *J Radiat Res* 2011;52:199–207.
58. Gill S, Dang K, Fox C et al. Seminal vesicle intrafraction motion analysed with cinematic magnetic resonance imaging. *Radiat Oncol* 2014;9:174.
59. Gurney-Champion OJ, McQuaid D, Dunlop A et al. MRI-based assessment of 3D Intrafractional motion of head and neck cancer for radiation therapy. *Int J Radiat Oncol Biol Phys* 2018;100:306–16.
60. Tetar SU, Bruynzeel AME, Lagerwaard FJ et al. Clinical implementation of magnetic resonance imaging guided adaptive radiotherapy for localized prostate cancer. *Phys Imag Radiat Oncol* 2019;9:69–76.
61. Bruijnen T, Stemkens B, Terhaard CHJ et al. Intrafraction motion quantification and planning target volume margin determination of head-and-neck tumors using cine magnetic resonance imaging. *Radiother Oncol* 2019;130:82–8.